Monthly Notices
of the
ROYAL ASTRONOMICAL SOCIETY

Mon. Not. R. Astron. Soc. **402,** 2626–2636 (2010) doi:10.1111/j.1365-2966.2009.16079.x

Compressed sensing reconstruction of a string signal from interferometric observations of the cosmic microwave background

Y. Wiaux,[1,2]★ G. Puy[1] and P. Vandergheynst[1]

[1]*Institute of Electrical Engineering, Ecole Polytechnique Fédérale de Lausanne (EPFL), CH-1015 Lausanne, Switzerland*
[2]*Centre for Particle Physics and Phenomenology, Université catholique de Louvain (UCL), B-1348 Louvain-la-Neuve, Belgium*

Accepted 2009 November 20. Received 2009 November 17; in original form 2009 August 28

ABSTRACT

We propose an algorithm for the reconstruction of the signal induced by cosmic strings in the cosmic microwave background (CMB), from radio-interferometric data at arcminute resolution. Radio interferometry provides incomplete and noisy Fourier measurements of the string signal, which exhibits sparse or compressible magnitude of the gradient due to the Kaiser–Stebbins effect. In this context, the versatile framework of compressed sensing naturally applies for solving the corresponding inverse problem. Our algorithm notably takes advantage of a model of the prior statistical distribution of the signal fitted on the basis of realistic simulations. Enhanced performance relative to the standard CLEAN algorithm is demonstrated by simulated observations under noise conditions including primary and secondary CMB anisotropies.

Key words: techniques: image processing – techniques: interferometric – cosmic microwave background.

1 INTRODUCTION

Recent observations of the cosmic microwave background (CMB) and of the large-scale structure of the Universe have led to the definition of a concordance cosmological model. The analysis of the CMB temperature data over the whole celestial sphere from the *Wilkinson Microwave Anisotropy Probe* (*WMAP*) satellite experiment has been playing a dominant role in designing this precise picture of the Universe (Bennett et al. 2003; Spergel et al. 2003; Hinshaw et al. 2007; Spergel et al. 2007; Hinshaw et al. 2009; Komatsu et al. 2009). According to this model, the cosmic structures and the CMB originate from Gaussian adiabatic perturbations seeded in the early phase of inflation of the Universe. However, cosmological scenarios motivated by theories for the unification of the fundamental interactions predict the existence of topological defects, resulting from phase transitions at the end of inflation (Vilenkin & Shellard 1994; Hindmarsh 1995; Hindmarsh & Kibble 1995; Turok & Spergel 1990). These defects would have participated in the formation of the cosmic structures, also imprinting the CMB. Cosmic strings are a line-like version of such defects which are also predicted in the framework of fundamental string theory (Davis & Kibble 2005). As a consequence, the issue of their existence is a central question in cosmology today.

Cosmic strings are parametrized by a string tension μ, i.e. a mass per unit length, which sets the overall strength of a string network. Their main signature in the CMB is characterized by temperature steps along the string positions. This localized effect, known as the Kaiser–Stebbins (KS) effect (Kaiser & Stebbins 1984; Gott 1985), hence implies a non-Gaussian imprint of the string network in the CMB. The most numerous strings appear at an angular size of around 1° on the celestial sphere. CMB experiments with an angular resolution much below 1° are thus required in order to resolve the width of cosmic strings.

Experimental constraints have been obtained on a possible string contribution in terms of upper bounds on the string tension μ (Perivolaropoulos 1993; Bevis, Hindmarsh & Kunz 2004; Wyman, Pogosian & Wasserman 2005, 2006; Bevis et al. 2007; Fraisse 2007). In this context, even though observations largely fit with an origin of the cosmic structures in terms of adiabatic perturbations, room is still available for the existence of cosmic strings.

The observed CMB signal can be modelled as a linear superposition of a statistically isotropic but non-Gaussian string signal x proportional to an unknown string tension, with statistically isotropic Gaussian noise g comprising the standard components of the CMB induced by adiabatic perturbations, as well as instrumental noise. In a first recent work (Hammond, Wiaux & Vandergheynst 2009) we developed an effective method for mapping the string network potentially imprinted in CMB temperature data, in the perspective of forthcoming arcminute resolution experiments performing a mapping of planar patches of the sky in real space, with standard radiometers. We took a Bayesian approach to this denoising problem, based on statistical models for both the string signal and the noise. The denoising is done in the wavelet domain, using a steerable wavelet transform well adapted for representing the strongly

★E-mail: yves.wiaux@epfl.ch

© 2010 The Authors. Journal compilation © 2010 RAS

oriented features present in the string signal. We showed that the string signal coefficients are well modelled by generalized Gaussian distributions (GGDs), which are fitted at each wavelet scale using a training simulation borrowed from the set of realistic string simulations recently produced by Fraisse et al. (2008).

In this work, we aim at extending the approach described above to the reconstruction of a string signal from radio-interferometric observations of the CMB probing small patches of the celestial sphere at the same arcminute resolution. Under the most standard assumptions, radio interferometers provide a noisy and incomplete Fourier coverage of the planar signal. In these terms, the signal reconstruction amounts to solving an ill-posed inverse problem encompassing both denoising and deconvolution. Relying on the KS effect in the CMB, the string network itself can be mapped by the magnitude of the gradient ∇x of the string signal, which is very sparse or compressible in nature, with significant amplitudes only along the strings themselves.

The theory of compressed sensing offers a new framework for solving an ill-posed inverse problem when the signals are sparse or compressible (Candès 2006; Candès, Romberg & Tao 2006a,b; Donoho 2006; Baraniuk 2007; Donoho & Tanner 2009). A band-limited signal may be expressed as the N^2-dimensional vector of its values sampled at the Nyquist–Shannon rate. By definition, a signal is sparse in some basis if its expansion contains only a small number $K \ll N^2$ of non-zero coefficients. More generally, it is compressible if its expansion only contains a small number of significant coefficients, i.e. if a large number of its coefficients bear a negligible value. The theory of compressed sensing demonstrates that, for sparse or compressible signals, a small number $M \ll N^2$ of random measurements, in a sensing basis incoherent with the sparsity basis, will suffice for an accurate and stable reconstruction of the signals. The mutual coherence between two bases may be defined as the maximum complex modulus of the scalar product between unit-norm vectors of the two bases. A random selection of Fourier measurements of a signal sparse in real space or in its gradient is particular examples of good sensing procedures. In this framework, the reconstruction of the signals may be approached in different ways, but all of them encompass a regularization of the ill-posed inverse problem by the introduction of a sparsity or compressibility constraint. In a second recent work (Wiaux et al. 2009a), we presented results showing that compressed sensing offers powerful image reconstruction techniques for radio-interferometric data, which are stable relative to noise as well as stable relative to non-exact sparsity, i.e. compressibility of the signals. These techniques are based on global minimization problems, which are solved by convex optimization algorithms (Combettes & Pesquet 2007; van den Berg & Friedlander 2008). We particularly illustrated the versatility of the scheme relative to the inclusion of specific prior information on the signal in the minimization problems.

We here wish to apply these results for the reconstruction of a string signal in the CMB. As for the denoising algorithm proposed in Hammond et al. (2009), the reconstruction algorithm that we present may be considered as a modular component of a larger data analysis. It may notably find use as a pre-processing step for other methods for cosmic string detection based on explicit edge detection (Jeong & Smoot 2005; Lo & Wright 2005; Amsel, Berger & Brandenberger 2007; Danos & Brandenberger 2008). Our reconstruction algorithm is tested under different conditions with astrophysical noise components including various contributions to the standard components of the CMB, i.e. primary and secondary anisotropies. Our analyses rely on the set of realistic string simulations recently produced by Fraisse et al. (2008).

The remainder of this paper is organized as follows. In Section 2, we discuss the string signal and noise in the CMB. In Section 3, we describe the inverse problem posed in the context of radio interferometry. In Section 4, we define the minimization problems to be solved for signal reconstruction in the context of compressed sensing, notably relying on a prior statistical model of the string signal fitted from simulations. In Section 5, we describe our numerical analyses and results. We finally conclude in Section 6.

2 STRING SIGNAL AND NOISE

In this section, we describe the string signal in the CMB as well as the astrophysical noise made up of the standard primary and secondary anisotropies. We also describe the numerical simulations used for our subsequent analyses.

2.1 String signal

In an inflationary cosmological model, the phase transitions responsible for the formation of a cosmic string network occur after the end of inflation so as to produce observable defects. From the epoch of last scattering until today, the cosmic string network continuously imprints the CMB. The so-called scaling solution for the string network implies that the most numerous strings are imprinted just after last scattering and have a typical angular size of around 1°, of the order of the horizon size at that time (Vachaspati & Vilenkin 1984; Albrecht & Turok 1985; Kibble 1985; Bennet 1986; Albrecht & Turok 1989; Bennet & Bouchet 1989; Allen & Shellard 1990; Bennet & Bouchet 1990). Longer strings are also imprinted in the later stages of the Universe evolution, but in smaller number, according to the number of corresponding horizon volumes required to fill the sky.

The main signature of a cosmic string in the CMB is described by the KS effect according to which a temperature step is induced along the string position. The relative amplitude of this step is given by

$$\frac{\delta T}{T} = (8\pi\gamma\beta)\,\rho, \tag{1}$$

where $\beta = v/c$ and $\gamma = (1-\beta^2)^{-1/2}$ with v standing for the string velocity transverse to the line of sight and c for the speed of light, and where ρ is a dimensionless parameter uniquely associated with the string tension μ through

$$\rho = \frac{G\mu}{c^2}, \tag{2}$$

with G standing for the gravitational constant. In the following, we call ρ the string tension.

On small angular scales, realistic simulations can be produced by stacking CMB maps induced in different redshift ranges between last scattering and today. The simulations that we use in this work have been produced by this technique (Bouchet, Bennet & Stebbins 1988; Fraisse et al. 2008). The string signal is understood as a realization of a statistically isotropic but non-Gaussian process on the celestial sphere with an overall amplitude rescaled by the string tension ρ and characterized by a nearly scale-free angular power spectrum: $C_l^{(x)}(\rho) = \rho^2 C_l^{(x)}$, where the positive integer index l stands for the angular frequency index on the sphere. An analytical expression of this spectrum was provided for l larger than a few hundreds by Fraisse et al. (2008), on the basis of their simulations.

© 2010 The Authors. Journal compilation © 2010 RAS, MNRAS **402,** 2626–2636

We consider radio-interferometric CMB observations with a small field of view corresponding to an angular opening $L \in [0, 2\pi)$ on the celestial sphere. In this context, the small portion of the celestial sphere accessible is identified to a planar patch of size $L \times L$, and we may consider planar signals functions of a two-dimensional position vector $\boldsymbol{p}$. The corresponding spatial frequencies may be denoted as two-dimensional vectors $\boldsymbol{k}$ with a radial component given by the norm k of the vector. In this Euclidean limit, the radial component identifies with the angular frequency on the celestial sphere, below some band limit B set by the resolution of the interferometer under consideration: $l = k < B$. For k larger than a few hundred, the nearly scale-free planar power spectrum of the string signal $x(\boldsymbol{p})$ reads as

$$P^{(x)}(k, \rho) = \rho^2 P^{(x)}(k), \tag{3}$$

with $P^{(x)}(k) = C_l^{(x)}$ for $l = k$.

The observed CMB signal can be understood as a linear superposition of the string signal and statistically isotropic noise of astrophysical and instrumental origin $g(\boldsymbol{p})$ with some angular power spectrum $C_l^{(g)}$. In the Euclidean limit, the corresponding planar power spectrum for the noise $g(\boldsymbol{p})$ may be written as $P^{(g)}(k) = C_l^{(g)}$ for $l = k$. Let us note that we consider zero mean signals, identifying perturbations around statistical means.

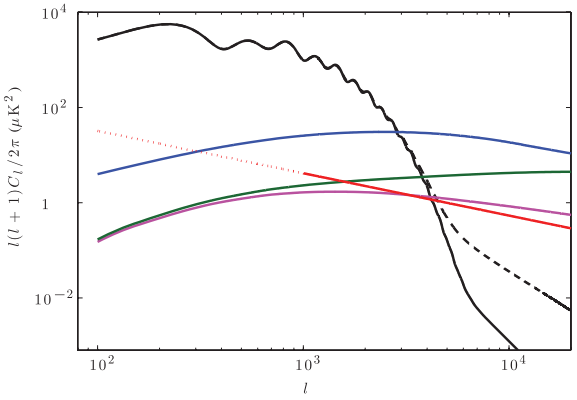

Figure 1. Angular power spectra of the string signal and noise (borrowed from Fraisse et al. 2008) as functions of the angular frequency in the range $l \in [10^2, 2 \times 10^4]$ in $\log_{10}$–$\log_{10}$ axes scaling. The spectrum of the string signal is represented for a string tension $\rho = 2 \times 10^{-7}$ in terms of its analytical expression valid at high angular frequencies (red straight line). The noise spectra (ordered by decreasing amplitude at low angular frequencies) are the primary CMB anisotropies (black solid line) and the gravitational lensing correction (black dashed line), the thermal SZ effect in the Rayleigh–Jeans limit (blue solid line), the non-linear kinetic SZ effect (green solid line) and the Ostriker–Vishniac effect (magenta solid line).

2.2 Astrophysical noise

Current CMB experiments achieve an angular resolution on the celestial sphere of the order of 10 arcmin, corresponding to a limit angular frequency not far above $B \simeq 10^3$. At such resolutions, the standard components of the CMB primarily contain the statistically isotropic and Gaussian primary anisotropies induced by adiabatic perturbations at last scattering. In this context, any possible string signal is confined to amplitudes largely dominated by these primary anisotropies. The constraints mainly come from a best-fitting analysis of the angular power spectrum of the overall CMB signal in the *WMAP* temperature data (Perivolaropoulos 1993; Bevis et al. 2004; Wyman et al. 2005, 2006; Bevis et al. 2007; Fraisse 2007). The tightest of these constraints (Fraisse 2007) gives the following upper bound at the 68 per cent confidence level:

$$\rho \leq \rho^{(\mathrm{exp})} = 2.1 \times 10^{-7}. \tag{4}$$

Forthcoming experiments will provide access to higher angular resolution. Among other instruments, radio interferometers such as the Arcminute Microkelvin Imager will probe the CMB at angular resolutions below 1 arcmin (Jones 2002; Barker et al. 2006; Zwart et al. 2008). At these resolutions, the secondary CMB anisotropies induced by interaction of CMB photons with the evolving Universe after last scattering will dominate the primary anisotropies and must be accounted for.

The primary anisotropies exhibit exponential damping at high angular frequencies. This contrasts with the slow decay of the nearly scale-free angular power spectrum of the string signal, which thus dominates over the primary anisotropies at high enough angular frequencies. The secondary anisotropies include gravitational effects such as the Integrated Sachs–Wolfe (ISW) effect, the Rees–Sciama (RS) effect and gravitational lensing, as well as re-scattering effects such as the thermal and kinetic Sunyaev–Zel'dovich (SZ) effects. The SZ effects dominate these secondary anisotropies (Sunyaev & Zel'dovich 1980; Komatsu & Seljak 2002; Fraisse et al. 2008). The ISW and RS effects associated with the time evolution of the standard gravitational potentials can be neglected at these angular frequencies. One may thus restrict the secondary anisotropies considered in the noise to the linear (Ostriker–Vishniac) and non-linear kinetic SZ effects as well as the thermal SZ effect. The SZ effects are actually non-Gaussian, spatially dependent, and the kinetic and thermal effects are correlated. As a simplifying assumption, we treat these two effects as two independent statistically isotropic Gaussian noise components. The effect of gravitational lensing is very small relative to the SZ effects, but we still take it into account as a correction to the angular power spectrum of the primary anisotropies.

At arcminute resolution, the thermal and kinetic SZ effects have standard deviations of around 10 and 5 μK, respectively. They also have a slow decay at high angular frequencies and will dominate the string signal for string tension values below the current experimental upper bound. Arcminute CMB experiments are in fact primarily dedicated to the detection of these secondary anisotropies. Unlike the other effects considered, which have the same blackbody spectrum as the primary anisotropies, the thermal SZ effect on the CMB temperature depends on the frequency of observation. Its amplitude decreases between the Rayleigh–Jeans limit (null frequency) and 217 GHz where it is expected to vanish, before increasing again at higher frequencies. Fig. 1 represents the angular power spectra as functions of the angular frequency l, for a string signal with string tension $\rho = 2 \times 10^{-7}$, for the primary CMB anisotropies and the correction due to gravitational lensing, for the Ostriker–Vishniac and the non-linear kinetic SZ effects and for the thermal SZ effect in the Rayleigh–Jeans limit. These spectra are explicitly borrowed from Fraisse et al. (2008).

In this context, the performance of the reconstruction algorithm to be defined will be studied in the following limits. In a first noise condition, we will consider the secondary anisotropies as a statistically isotropic Gaussian noise, with the power spectrum given by the Rayleigh–Jeans limit, that is added to the primary anisotropies. In a second noise condition, we will also assume an observation frequency of around 217 GHz taking advantage of the frequency dependence of the thermal SZ effect, and include in the noise secondary anisotropies in absence of this effect. This is equivalent to including only the kinetic SZ effect and gravitational lensing in

the secondary anisotropies. Instrumental noise is considered to be negligible and simply discarded. These two different noise conditions are, respectively, denoted as SA + tSZ (secondary anisotropies with thermal SZ effect) and SA-tSZ (secondary anisotropies without thermal SZ effect) in the following. Analysing these limits can reveal to what extent the kinetic and thermal SZ effects hamper the reconstruction of the string signal, as a function of the string tension. In a third noise condition, the reconstruction performance will also be examined in the limit where the noise only includes primary anisotropies, neglecting even instrumental noise and assuming that secondary anisotropies have been correctly separated. This case is denoted as PA-IN (primary anisotropies without instrumental noise) and will be studied in order to understand the behaviour of the reconstruction algorithm in ideal conditions.

For the sake of our analyses, foreground emissions such as Galactic dust or point sources (Kosowsky 2006) are disregarded.

2.3 Numerical simulations

We use simulations of the string signal borrowed from the set of realistic simulations produced by Fraisse et al. (2008). The specific simulations considered are defined on planar patches of size $L \times L$ for a field of view defined by an angular opening $L = 0.^{\circ}9$. The finite size of the patch induces a discretization of the spatial frequencies which may be defined on a grid with $N \times N$ uniformly sampled points $\boldsymbol{k}_i$ with $1 \leq i \leq N^2$, below some band limit B. The original maps are sampled at the Nyquist–Shannon rate on grids with $N \times N$ uniformly sampled points $\boldsymbol{p}_i$ with $1 \leq i \leq N^2$. We consider here samples with $N = 128$ so that the corresponding pixels have an angular size of around 0.42 arcmin, with a band limit $B \simeq 2.5 \times 10^4$ on each component of the spatial frequencies.

For each noise component, a simulation may easily be produced by taking the Fourier transform of Gaussian white noise, renormalizing each Fourier coefficient by the square root of the corresponding power spectrum and inverting the Fourier transform (Rocha et al. 2005). In each noise condition considered, an overall noise simulation is obtained by simple superposition of the required independent components simulated. The power spectrum of the noise $P^{(g)}(k)$ is the sum of the individual spectra.

Our approach for signal reconstruction notably relies on the introduction of specific statistical prior information on the signal in the regularization of the ill-posed inverse problem. A number of 64 simulations of the string signal x are used as training data for fitting a prior statistical model for the gradient of the signal. Only one additional simulation is reserved for testing the algorithm. In all noise conditions considered and for each string tension, this test string signal simulation is combined with 30 independent realizations of the noise in order to produce multiple test simulations. For illustration, Fig. 2 represents the test simulation of the string signal and one simulation of the noise, as well as corresponding maps of the magnitude of the gradient.

Note that due to the finite size of the simulations, different string signal simulations exhibit slightly different estimated power spectra. For simplicity of our argument though both training and test simulations have been normalized so as to exhibit the same total power for the same string tension (see Hammond et al. 2009 for more details).

3 INTERFEROMETRIC INVERSE PROBLEM

In this section, we describe the ill-posed inverse problem posed for reconstruction of the string signal in the context of radio-interferometric observations of the CMB. We also describe a modified inverse problem including a whitening operation on the measured visibilities and discuss basic ideas for signal reconstruction.

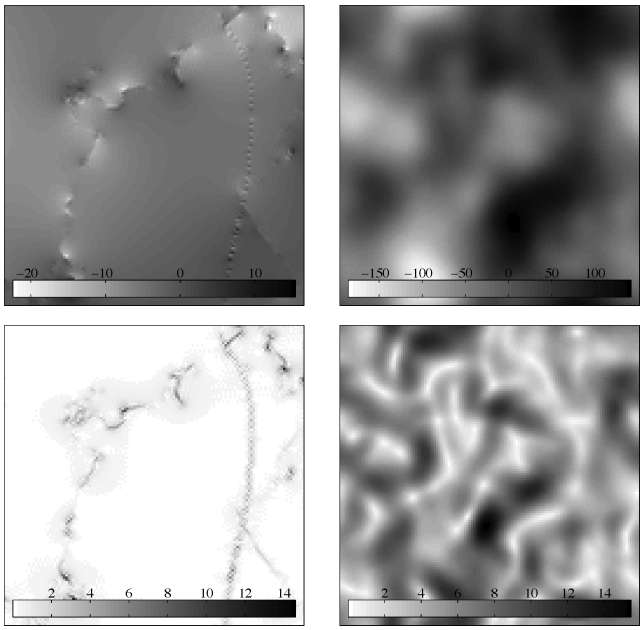

Figure 2. Simulated temperature maps (in μK) of the string signal in the CMB and of its magnitude of gradient for a tension $\rho = 2 \times 10^{-7}$ are represented in the top and bottom left-hand panels, respectively. Temperature maps of the primary CMB anisotropies, i.e. the noise in the PA-IN condition, and of its magnitude of gradient are represented in the top and bottom right-hand panels, respectively.

3.1 Inverse problem

Aperture synthesis in radio interferometry is a powerful technique in radio astronomy dating back to more than 60 years ago (Ryle & Vonberg 1946; Blythe 1957; Ryle, Hewish & Shakeshaft 1959; Ryle & Hewish 1960; Thompson, Moran & Swenson 2004). In this context, the small portion of the celestial sphere around the pointing direction tracked by a radio telescope array during observation defines the original real planar signal or image probed x. The field of view observed is limited by a primary beam represented by a function A with values in the range [0, 1]. Each telescope pair at one instant of observation identifies a baseline defined as the relative position between the two telescopes. With each baseline is associated one measurement called visibility. In the simplest setting, one also considers baselines with a negligible component in the pointing direction of the instrument. Under this additional assumption, if the signal is made up of incoherent sources, each visibility corresponds to the value of the Fourier transform of the signal multiplied by the primary beam at a spatial frequency $\boldsymbol{k}$ identified by the components of the baseline in the plane of the signal.

We assume that the spatial frequencies $\boldsymbol{k}$ probed by all telescope pairs during the observation belong to the discrete grid of points $\boldsymbol{k}_i$ (see Wiaux et al. 2009a for more details). The Fourier coverage provided by the $M/2$ spatial frequencies $\boldsymbol{k}_\mathrm{b}$ probed, with $1 \leq b \leq M/2$, can simply be identified by a binary mask in the Fourier plane equal to 1 for each spatial frequency probed and 0 otherwise. The visibilities measured may be denoted by a vector of $M/2$ complex Fourier coefficients $\boldsymbol{y} \in \mathbb{C}^{M/2} \equiv \{y_\mathrm{b} \equiv y(\boldsymbol{k}_\mathrm{b})\}_{1 \leq b \leq M/2}$. Formally, the visibilities may equivalently be denoted by a vector of M real

© 2010 The Authors. Journal compilation © 2010 RAS, MNRAS **402,** 2626–2636

measures $\boldsymbol{y} \in \mathbb{R}^M \equiv \{y_r\}_{1\leq r\leq M}$ consisting of the real and imaginary parts of the complex measures. In this discrete setting, the Fourier coverage is in general incomplete in the sense that the number of real constraints M is smaller than the number of unknowns N^2: $M < N^2$. An ill-posed inverse problem is thus defined for the reconstruction of the signal, seen as a vector of real sampled values $\boldsymbol{x} \in \mathbb{R}^{N^2} \equiv \{x(\boldsymbol{p}_i)\}_{1\leq i\leq N^2}$, from the measured visibilities $\boldsymbol{y}$. In the context of our analysis, the noise affecting the signal consists in the vector of real sampled values for the standard CMB components $\boldsymbol{g} \in \mathbb{R}^{N^2} \equiv \{g(\boldsymbol{p}_i)\}_{1\leq i\leq N^2}$. The inverse problem therefore reads as

$$\begin{aligned} \boldsymbol{y} \equiv \Phi\boldsymbol{x} + \boldsymbol{n} \qquad & \text{with} \qquad \Phi \equiv \mathbf{MFA} \\ & \text{and with} \qquad \boldsymbol{n} \equiv \Phi\boldsymbol{g}, \end{aligned} \tag{5}$$

where the measurement matrix $\Phi \in \mathbb{C}^{(M/2)\times N^2}$ identifies the complete linear relation between the signal and the visibilities. The matrix $\mathbf{A} \in \mathbb{R}^{N^2\times N^2} \equiv \{A_{ij} \equiv A(\boldsymbol{p}_i)\delta_{ij}\}_{1\leq i,j\leq N^2}$ is the diagonal matrix implementing the primary beam. The unitary matrix $\mathbf{F} \in \mathbb{C}^{N^2\times N^2} \equiv \{F_{ij} \equiv \mathrm{e}^{-\mathrm{i}\boldsymbol{k}_i\cdot\boldsymbol{x}_j}/N\}_{1\leq i,j\leq N^2}$ implements the discrete Fourier transform providing the Fourier coefficients. The matrix $\mathbf{M} \in \mathbb{R}^{(M/2)\times N^2} \equiv \{M_{bj}\}_{1\leq b\leq M/2;1\leq j\leq N^2}$ is the rectangular binary matrix implementing the mask characterizing the interferometer. It contains only one non-zero value on each line, at the index of the Fourier coefficient corresponding to each of the spatial frequencies $\boldsymbol{k}_\mathrm{b}$ probed. Neglecting small correlations introduced between spatial frequencies by the primary beam, the power spectrum of the noise $\boldsymbol{g}$ is none the less modified as $P^{(Ag)}(k) = |\widehat{A}(k)|^2 P^{(g)}(k)$. The noise $\boldsymbol{n} \in \mathbb{C}^{M/2} \equiv \{n_\mathrm{b}\}_{1\leq b\leq M/2}$ affecting the visibilities is Gaussian noise with different variances $P^{(Ag)}(k_\mathrm{b})$ for different components n_b. Let us recall that $\boldsymbol{g}$ is real so that the components of $\boldsymbol{n}$ are independent only when we assume that the mask $\mathbf{M}$ contains no pair of antipodal spatial frequencies $\{\boldsymbol{k}_\mathrm{b}, -\boldsymbol{k}_\mathrm{b}\}$. For each such pair, the two corresponding noise components are complex conjugate of one another. In this work $M/2$ denotes the number of independent complex visibilities, while $M_0/2$, with $M_0 \geq M$, will stand for the total number of complex visibilities including possible pairs of antipodal spatial frequencies.

3.2 Whitening

The measurement matrix may be augmented by a whitening operation which will be useful in a reconstruction perspective. It consists in dividing each measured visibility y_b by the standard deviation of the real and imaginary parts of the corresponding noise component n_b. This operation is simply implemented in terms of the diagonal matrix $\mathbf{W} \in \mathbb{R}^{(M/2)\times(M/2)} \equiv \{W_{bb'} \equiv [P^{(Ag)}(k_\mathrm{b})/2]^{1/2}\delta_{bb'}\}_{1\leq b,b'\leq(M/2)}$. This gives rise to the modified inverse problem

$$\begin{aligned} \tilde{\boldsymbol{y}} \equiv \tilde{\Phi}\boldsymbol{x} + \tilde{\boldsymbol{n}} \qquad & \text{with} \qquad \tilde{\Phi} \equiv \mathbf{WMFA} \\ & \text{and with} \qquad \tilde{\boldsymbol{n}} \equiv \tilde{\Phi}\boldsymbol{g}, \end{aligned} \tag{6}$$

where the whitened visibilities $\tilde{\boldsymbol{y}} \in \mathbb{C}^{M/2} \equiv \{\tilde{y}_\mathrm{b} \equiv \tilde{y}(\boldsymbol{k}_\mathrm{b})\}_{1\leq b\leq M/2}$ are now affected by identically distributed independent (i.i.d.) Gaussian noise with unit variance of the real and imaginary parts of each component n_b, i.e. white Gaussian noise.

For each test simulation, the visibilities are computed in accordance with relation (5). The primary beam A considered for our observational set-up is a Gaussian function with a full width at half-maximum (FWHM) equal to the angular opening of the field of view: FWHM $= L$. The function has a maximum value equal to unity. Two Fourier coverages are considered independently, defined by masks made up of a random selection of M_0 spatial frequencies (see Wiaux et al. 2009a for more details) with either 25 or 50 per cent of the Fourier plane probed up to the band limit B. Note that, after discarding redundant visibilities associated with pairs of antipodal spatial frequencies in the two masks considered, these two percentages, respectively, correspond to selections of M spatial frequencies with 21.7 and 37.4 per cent. The primary beam and the mask for a Fourier coverage of 25 per cent are illustrated in Fig. 3. The visibilities are also whitened in accordance with relation (6) by the introduction of the suitable matrix $\mathbf{W}$ in each noise condition.

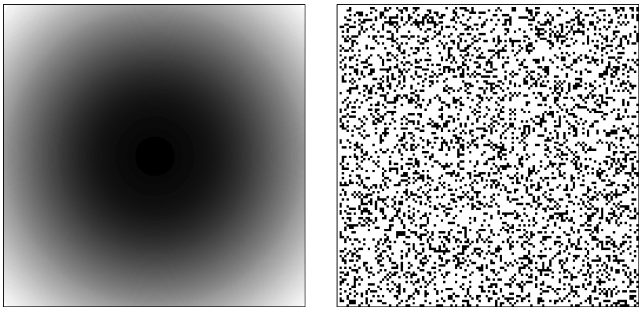

Figure 3. A map of the primary beam considered is represented in the left-hand panel, with darkness increasing with the value of the function A in the range $[0, 1]$. A map of the mask made up of a random selection of 25 per cent of the spatial frequencies up to the band limit in the Fourier plane is represented in the right-hand panel, with a unit value at the position of the selected frequencies identified by black points, and zero otherwise.

3.3 Reconstruction basics

In the perspective of the reconstruction of the signal $\boldsymbol{x}$, relation (6) represents the measurement constraint. Considering a candidate reconstruction $\bar{\boldsymbol{x}}$, the residual noise reads as $\bar{\boldsymbol{n}} \in \mathbb{C}^{M/2} \equiv \{\bar{n}_\mathrm{b}\}_{1\leq b\leq M/2} \equiv \tilde{\boldsymbol{y}} - \tilde{\Phi}\bar{\boldsymbol{x}}$. The residual noise level estimator, defined as twice the negative logarithm of the likelihood associated with $\bar{\boldsymbol{x}}$, simply reads as

$$\chi^2(\boldsymbol{y}, \Phi, \bar{\boldsymbol{x}}) \equiv 2\sum_{b=1}^{M/2} \frac{\left|y_\mathrm{b} - (\Phi\bar{\boldsymbol{x}})_\mathrm{b}\right|^2}{P^{(Ag)}(k_\mathrm{b})} \equiv ||\bar{n}||_2^2. \tag{7}$$

The notation $|\cdot|$ for a scalar stands for the complex modulus when applied to a complex number and for the absolute value when applied to a real number. The ℓ_2 norm of the residual noise is the standard norm of the corresponding vector: $||\bar{\boldsymbol{n}}||_2 \equiv (\sum_{b=1}^{M/2} |\bar{n}_\mathrm{b}|^2)^{1/2}$. This noise level estimator follows a χ^2 distribution with M degrees of freedom. Typically, this estimator should be minimized by the good candidate reconstruction. The measurement constraint on the reconstruction may be defined as a bound $\chi^2(\boldsymbol{y}, \Phi, \bar{\boldsymbol{x}}) \leq \epsilon^2$, with ϵ^2 corresponding to some suitable large percentile of the χ^2 distribution in order to avoid noise over-fitting.

In this context, many signals may formally satisfy the measurement constraint. A regularization scheme that encompasses enough prior information on the original signal is needed in order to find a unique solution. All image reconstruction algorithms will differ through the kind of regularization considered.

First, the simplest possible reconstruction procedure would consist in assuming that the non-probed spatial frequencies have a null value and simply inverting the Fourier transform after dividing each visibility by the variance of the noise in order to enhance the signal-to-noise ratio. This reconstruction can be written as $\boldsymbol{x}_0 \propto (\mathbf{WMF})^\dagger\tilde{\boldsymbol{y}}$, where the notation $\cdot^\dagger$ stands for the

conjugate transpose operation. This map simply identifies with the convolution of the original signal and noise $\mathbf{A}(\boldsymbol{x}+\boldsymbol{g})$ by a beam $(\mathbf{F}^\dagger\mathbf{M}^\dagger\mathbf{W}^2\mathbf{M}\mathbf{F})\boldsymbol{\delta_0}$, where $\boldsymbol{\delta_0}$ stands for a spike at the centre of the field of view: $\boldsymbol{\delta_0} \in \mathbb{R}^{N^2} \equiv \{\delta_{i_0 j}\}_{1\leq j\leq N^2}$, with i_0 identifying the central pixel. In the standard vocabulary of radio interferometry, the beam is called the dirty beam and the convolved map is called the dirty map in recognition of its visual appearance contrasting with the original signal. A normalization constant needs to be chosen so as to get a unit central value of the beam. In other words, no denoising or deconvolution is performed by this simple procedure that we call INVERT. The only important operation in this reconstruction is the enhancement of the signal-to-noise ratio by the matrix $\mathbf{W}^2$.

Secondly, the standard CLEAN algorithm is essentially a Matching Pursuit algorithm (Mallat & Zhang 1993; Mallat 1998) which performs the deconvolution by iterative removal of the dirty beam, thus leading from the dirty map to a clean map (Högbom 1974; Schwarz 1978; Thompson et al. 2004). Formally, the algorithm should be stopped when the above χ^2 constraint is satisfied.

4 COMPRESSED SENSING RECONSTRUCTION

In this section, we describe the standard global Total Variation minimization problem (TV_ϵ) for the reconstruction of the string signal in the context of compressed sensing. We model the prior statistical distribution of the gradient of the string signal with a GGD, fitted on the basis of the training simulations. We also propose to enhance the TV_ϵ problem on the basis of this statistical prior information, hence defining a Statistical Total Variation (STV_ϵ) minimization problem. We finally propose a power spectral model (PSM) used for independent estimation of the string tension, which may notably be useful for accelerating the convergence of the iterative algorithms solving the minimization problems.

4.1 TV_ϵ problem

For the reconstruction of a signal of sparsity K, the theory of compressed sensing proves that the number M of random measurements required, in a sensing basis incoherent with the sparsity basis, roughly scales with the sparsity, well below the number of samples N^2 of the signal at the Nyquist–Shannon rate: $M \propto K \ll N^2$ (Candès 2006; Candès 2008; Candès et al. 2006b). In the case of radio-interferometric data, the measurements are assumed to be random Fourier samples which represent a good sensing procedure for a string signal x exhibiting sparse magnitude of the gradient ∇x. In this case, in the presence of i.i.d. Gaussian noise, the so-called Total Variation minimization problem (TV_ϵ) applies (Candès et al. 2006a), which corresponds to the minimization of the TV norm of the real signal under a χ^2 constraint on the candidate reconstruction $\bar{\boldsymbol{x}}$:

$$\min_{\bar{\boldsymbol{x}}\in\mathbb{R}^{N^2}} ||\bar{\boldsymbol{x}}||_{\mathrm{TV}} \quad \text{subject to} \quad \chi^2(\boldsymbol{y}, \Phi, \bar{\boldsymbol{x}}) \leq \epsilon^2. \tag{8}$$

The vector of sample values of the magnitude of the gradient associated with the vector $\boldsymbol{x}$ is denoted as $\nabla\boldsymbol{x} \in \mathbb{R}^{N^2} \equiv \{\nabla x(\boldsymbol{p}_i)\}_{1\leq i\leq N^2}$. By definition, the TV norm of a signal is the ℓ_1 norm of the magnitude of its gradient, i.e. $||\bar{\boldsymbol{x}}||_{\mathrm{TV}} = ||\boldsymbol{\nabla}\bar{\boldsymbol{x}}||_1 \equiv \sum_{i=1}^{N^2} |\nabla x(\boldsymbol{p}_i)|$. We set ϵ^2 to be the 99th percentile of the χ^2 distribution.

The iterative algorithm considered for solving this convex optimization problem is based on the Douglas–Rachford splitting method (Combettes & Pesquet 2007; Fadili & Starck 2009) in the framework of proximal operator theory (Moreau 1962).

4.2 Signal prior

In a Bayesian perspective, the minimization of the TV norm of the signal amounts to assuming that the signal gradient follows a Laplacian distribution with no spatial correlations and to minimizing the negative logarithm of this prior distribution, i.e. to maximizing the distribution, subject to the χ^2 constraint. This promotes compressibility in a generic sense. A Laplacian distribution is indeed more peaked and more heavy-tailed than a Gaussian prior for example. However, with realistic simulations of the string signal at hand one can study more precisely the signal distribution. In this perspective, the signal gradient can be modelled at each sample point by the positive tail of a GGD:

$$\mathcal{P}(\nabla x|\rho) = \frac{q}{2\rho s\Gamma\left(q^{-1}\right)} \mathrm{e}^{-|\frac{\nabla x}{\rho s}|^q}, \tag{9}$$

where Γ is the gamma function and q and ρs are, respectively, called shape and scale parameters. The shape parameter q can be considered as a continuous measure of the compressibility of the underlying distribution. Setting $q = 2$ recovers a Gaussian distribution, and $q = 1$ recovers a Laplacian distribution. Letting q approach 0 yields compressible distributions. This parameter determines the kurtosis $\kappa^{(\nabla x)}$, i.e. the ratio of the fourth central moment to the square of the variance (second central moment), by

$$\kappa^{(\nabla x)} = \frac{\Gamma\left(5q^{-1}\right)\Gamma\left(q^{-1}\right)}{\left[\Gamma\left(3q^{-1}\right)\right]^2}. \tag{10}$$

By nature, this kurtosis is independent of the string tension ρ. The scale parameter ρs is linearly proportional to the standard deviation $\sigma^{(\nabla x)}(\rho)$ of the distribution. The corresponding variance reads as

$$\left[\sigma^{(\nabla x)}(\rho)\right]^2 = \rho^2 \frac{\Gamma\left(3q^{-1}\right)}{\Gamma\left(q^{-1}\right)} s^2. \tag{11}$$

The shape and scale parameters are estimated by a moment method on the aggregate of the magnitude of the gradient of the 64 test simulations. The values with two significant figures are $\widehat{q} = 0.42$ and $\widehat{s} = 2.3 \times 10^5$, respectively. The shape parameter value shows that the signal gradient exhibits a much more compressible gradient than a generic Laplacian distribution. Fig. 4 shows the positive tail of the modelled prior GGD distribution $\mathcal{P}(\nabla x|\rho)$ for a string tension $\rho = 2 \times 10^{-7}$. The GGD is superimposed on the

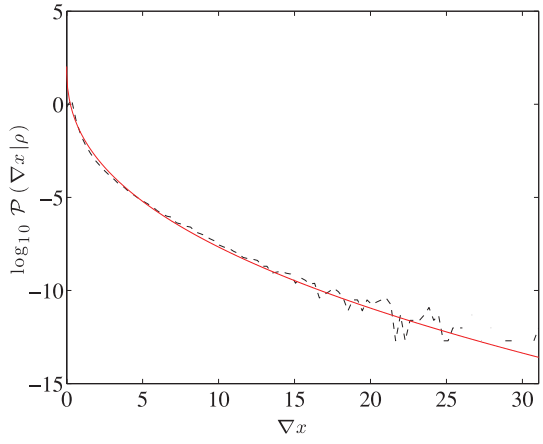

Figure 4. Positive tail of modelled prior GGD distribution $\mathcal{P}(\nabla x|\rho)$ for a string tension $\rho = 2 \times 10^{-7}$. The GGD is superimposed on the histogram of the aggregate of the magnitude of the gradient of the 64 test simulations.

© 2010 The Authors. Journal compilation © 2010 RAS, MNRAS **402,** 2626–2636

histogram of the aggregate of the magnitude of the gradient of the 64 test simulations. Qualitatively, we see that the prior distribution is well modelled by a GGD.

4.3 STV$_\epsilon$ problem

Accounting for the specific statistical prior information in the regularization of the inverse problem should enhance the reconstruction performance, beyond the standard TV$_\epsilon$ minimization. In the Bayesian perspective discussed, we define a Statistical Total Variation (STV$_\epsilon$) minimization problem that consists in minimizing the logarithm of the GGD prior distribution modelled, subject to the χ^2 constraint

$$\min_{\bar{\boldsymbol{x}}\in\mathbb{R}^{N^2}} ||\bar{\boldsymbol{x}}||_{\mathrm{TV}}^{\widehat{q}} \quad \text{subject to} \quad \chi^2(\boldsymbol{y}, \Phi, \bar{\boldsymbol{x}}) \leq \epsilon^2. \tag{12}$$

Again, we set ϵ^2 to be the 99th percentile of the χ^2 distribution. Because $\widehat{q} < 1$ the problem is non-convex in nature, but a reweighted scheme allows convergence of the algorithm through iterations of simple TV$_\epsilon$ minimizations (Candès et al. 2006a).

Note that no prior knowledge of the string tension ρ is formally required for the reconstruction. However, we must acknowledge the fact that convergence appears to be faster when some prior estimation of ρ is used to renormalize $\bar{\boldsymbol{x}}$ in the minimization term of relations (8) and (12), as expected from relation (9). As discussed in Section 5, such an estimation of ρ will also define a threshold below which one should not expect good reconstruction of the string network. Our estimation procedure is described below.

4.4 String tension estimation

By the Bayes theorem, the posterior probability distribution for ρ given the measured visibilities $\mathcal{Q}(\rho|\boldsymbol{y})$ is simply obtained from the likelihood $\mathcal{L}(\boldsymbol{y}|\rho)$ and the prior probability distribution $\mathcal{P}(\rho)$ on ρ. For complete consistency, the likelihood should be calculated using the model established for the signal gradient and noise. However, while this model by construction accounts for the non-Gaussianity, i.e. sparsity of the string signal, it ignores the spatial correlations.

As in Hammond et al. (2009), we have observed that a likelihood yielding a precise localization of the string tension value can actually be obtained using a PSM. Such a model assumes that both the string signal and the noise arise from statistically isotropic Gaussian random processes, such that their Fourier coefficients are independent Gaussian variables. Under this model, as the string signal and noise are independent, the observed signal $\mathbf{A}(\boldsymbol{x} + \boldsymbol{g})$ has a power spectrum, as modified by the primary beam, of the form

$$P^{(A(x+g))}(k, \rho) = P^{(Ag)}(k) + P^{(Ax)}(k, \rho), \tag{13}$$

with $P^{(Ag)}(k)$ defined in Section 3.3 and similarly $P^{(Ax)}(k, \rho) = |\widehat{A}(k)|^2 P^{(x)}(k, \rho)$. In this setting, the likelihood can be computed easily in terms of the measured visibilities $\boldsymbol{y}$ as

$$\mathcal{L}(\boldsymbol{y}|\rho) = \prod_{b=1}^{M/2} \frac{1}{\pi P^{(A(x+g))}(k_\mathrm{b}, \rho)} \mathrm{e}^{-\frac{|y_\mathrm{b}|^2}{P^{(A(x+g))}(k_\mathrm{b}, \rho)}}. \tag{14}$$

The posterior probability distribution for ρ given the measured visibilities thus reads as

$$\mathcal{Q}(\rho|\boldsymbol{y}) = D^{-1}\mathcal{P}(\rho)\,\mathcal{L}(\boldsymbol{y}|\rho), \tag{15}$$

with normalization $D = \int \mathcal{P}(\rho)\mathcal{L}(\boldsymbol{y}|\rho)\,\mathrm{d}\rho$. We take the prior $\mathcal{P}(\rho)$ to be flat in an interval $\rho \in [0, \rho^{(\max)}]$, with an upper bound $\rho^{(\max)}$ large relative to the upper bound (4).

We define an estimation $\widehat{\rho}$ of the string tension as the expectation value of this posterior probability distribution:

$$\widehat{\rho} = E\left[\mathcal{Q}(\rho|\boldsymbol{y})\right]. \tag{16}$$

5 ANALYSES AND RESULTS

In this section, we first describe our numerical analyses, including the performance criteria of reconstruction, and discuss their results. We also compare the corresponding eye visibility thresholds on the string tension with the detectability threshold obtained on the basis of the PSM. We finally propose a small discussion of our results.

5.1 Analyses

The overall reconstruction is effective for mapping the string network if the magnitude of the gradient of the reconstructed signal closely resembles the magnitude of the gradient of the true string signal. A simple qualitative measure of the performance is given by whether the string network is visible in the magnitude of the gradient of the reconstructed signal. We define the eye visibility threshold as the minimum string tension around which the overall denoising and mapping by the magnitude of the gradient begin to exhibit string features visible by eye. We will augment this qualitative assessment of the reconstruction performance with three quantitative measures, namely the signal-to-noise ratio, the correlation coefficient and the kurtosis of the magnitude of the gradient of the reconstructed string signal re-multiplied by the primary beam. The kurtosis is known to be a good statistic for discriminating between models with and without cosmic strings (Moessner, Perivolaropoulos & Brandenberger 1994).

The signal-to-noise ratio is defined in terms of the original and reconstructed string signal gradients as

$$\mathrm{SNR}^{(\nabla Ax, \nabla A\bar{x})} = -20\log_{10}\frac{\sigma^{(\nabla Ax - \nabla A\bar{x})}}{\sigma^{(\nabla Ax)}}, \tag{17}$$

where $\sigma^{(\nabla Ax - \nabla A\bar{x})}$ and $\sigma^{(\nabla Ax)}$, respectively, stand for the standard deviations of the discrepancy signal $\nabla Ax - \nabla A\bar{x}$ and of the original signal ∇Ax. The standard deviations are estimated from the sample variances on the basis of the signal realizations concerned. With this definition, the SNR is measured in decibels (dB). We will consider that the reconstruction is meaningful in terms of signal-to-noise ratio for the values of ρ where this statistic is positive.

The correlation coefficient is also defined in terms of the original and reconstructed string signal gradients as

$$r^{(\nabla Ax, \nabla A\bar{x})} = \frac{\mathrm{cov}^{(\nabla Ax, \nabla A\bar{x})}}{\sigma^{(\nabla Ax)}\sigma^{(\nabla A\bar{x})}}, \tag{18}$$

where $\mathrm{cov}^{(\nabla Ax, \nabla A\bar{x})}$ stands for the covariance between ∇Ax and $\nabla A\bar{x}$, and $\sigma^{(\nabla Ax)}$ and $\sigma^{(\nabla A\bar{x})}$, respectively, stand for the standard deviations of the signals ∇Ax and $\nabla A\bar{x}$. The covariance and variances are again estimated from the sample covariance and variances on the basis of the signal realizations concerned. We will consider that the reconstruction is meaningful in terms of the correlation coefficient for the values of ρ where this statistic is also positive. Note that the variances and covariances discussed obviously depend on the string tension, but not their dimensionless ratios. For this reason, we have omitted this dependence in definitions (17) and (18).

Analogously, kurtoses of the magnitude of the gradient of the reconstructed string signal re-multiplied by the primary beam are estimated from the sample kurtoses on the basis of the signal realizations concerned. The kurtosis of the magnitude of the gradient

of a string signal as expected on the basis of our test string signal simulation takes the value $\kappa^{(\nabla Ax)} = 51$ with two significant numbers.

We compare the reconstruction results of the simple INVERT procedure and of the standard CLEAN algorithm with those of the TV_ϵ and STV_ϵ algorithms. Reconstructions are performed for string tensions equispaced in logarithmic scaling in the range $\log_{10}\rho \in [-9, -5]$, corresponding to ratio values of 1.0, 1.6, 2.5, 4.0 and 6.3 for ρ in each order of magnitude. For each string tension, each algorithm, each noise condition (PA-IN, SA-tSZ or SA + tSZ) and each coverage condition (25 or 50 per cent) analysed, we consider that the quantitative measures described above indicate effective performance when this performance is significant over the 30 corresponding simulations.

5.2 Results

In all noise and coverage conditions, the simple INVERT procedure is already effective at enhancing the visibility of strings by eye, thanks to the multiplication by $\mathbf{W}^2$ in Fourier space, but the resulting maps are dirty. The string tensions representing the eye visibility thresholds are listed in Table 1. These thresholds are well below the experimental upper bound in the noise condition PA-IN, while for the noise conditions SA-tSZ and SA + tSZ they are, respectively, of the same order and larger. This evolution is naturally due to the larger amount of noise at high spatial frequencies, where the signal gradient lives, in the presence of secondary anisotropies.

The eye visibility thresholds for CLEAN, TV_ϵ and STV_ϵ are the same as for INVERT. However, it clearly appears that these more evolved algorithms offer much better reconstructions. This can already be acknowledged by simple eye inspection, as illustrated in Fig. 5 for the magnitude of the gradient of the reconstructed signals re-multiplied by the primary beam in the noise condition PA-IN at 25 per cent and for a string tension $\rho = 1 \times 10^{-7}$. This qualitative assessment is confirmed by our quantitative measures for the reconstruction performance in all noise and coverage conditions and for all string tensions. Fig. 6 represents the SNR, correlation coefficient and kurtosis of the magnitude of the gradient of reconstructed string signals re-multiplied by the primary beam as functions of the string tension in all noise conditions and for a coverage of 25 per cent, for CLEAN, TV_ϵ and STV_ϵ. The corresponding curves for INVERT are actually not shown for readability reasons as they are very far from optimal values. In this context, the major interest of the analysis actually resides in the comparison of the standard CLEAN algorithm with the TV_ϵ and STV_ϵ algorithms.

First, the reconstructions illustrated in Fig. 5 seem very similar for CLEAN, TV_ϵ and STV_ϵ. Note, however, that the magnitude of the gradient of the original signal (not shown in the figure) re-multiplied by the primary beam lies roughly in the range $[0, 3.5]$. The range of amplitudes reported on the maps therefore indicates

Table 1. PSM detectability thresholds and eye visibility thresholds on the string tension, for each of the noise and coverage conditions considered. All values are given with two significant figures.

Noise	Coverage (per cent)	PSM detectability	Eye visibility
PA-IN	25	7.8×10^{-10}	1.6×10^{-9}
PA-IN	50	7.1×10^{-10}	1.0×10^{-9}
SA-tSZ	25	2.9×10^{-7}	6.3×10^{-7}
SA-tSZ	50	2.4×10^{-7}	4.0×10^{-7}
SA + tSZ	25	5.0×10^{-7}	1.0×10^{-6}
SA + tSZ	50	4.4×10^{-7}	6.3×10^{-7}

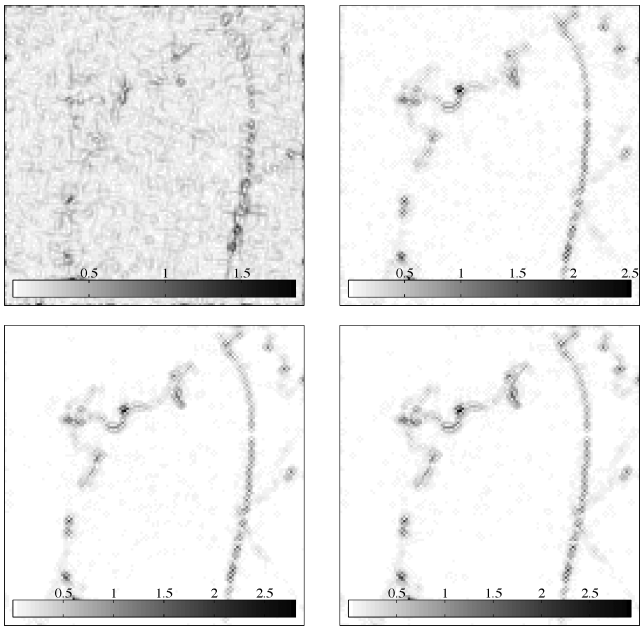

Figure 5. Magnitude of the gradient of reconstructed string signals re-multiplied by the primary beam, for a tension $\rho = 1 \times 10^{-7}$, in the noise condition PA-IN and for a coverage of 25 per cent. The reconstructions considered are those associated with the simple INVERT procedure (top left-hand panel), CLEAN (top right-hand panel), TV_ϵ (bottom left-hand panel) and STV_ϵ (bottom right-hand panel).

that the dynamic range of the reconstructions is better for TV_ϵ than for CLEAN, and even better for STV_ϵ. This is a generic behaviour that can be observed in all noise and coverage conditions and at all string tensions.

Secondly, as shown in Fig. 6 in all noise conditions and for a coverage of 25 per cent, the eye visibility thresholds identify with the string tension where the SNR and correlation coefficient get down to very small values, and the kurtosis exhibits a large variability over the 30 simulations around the expected value. This allows us to identify rigorously the eye visibility threshold as the string tension below which the algorithms are no longer effective at recovering the string network.

Thirdly, as also shown in Fig. 6 in all noise conditions and for a coverage of 25 per cent, the SNR and correlation coefficient are always significantly larger for TV_ϵ than for CLEAN. They are always at least as good for STV_ϵ as for TV_ϵ and often significantly larger. However, it appears that the kurtosis is less optimally recovered with TV_ϵ than with CLEAN. But the STV_ϵ approach regularizes the kurtosis significantly better than CLEAN in most cases.

Note that these last two conclusions also hold for a 50 per cent coverage, hence suggesting their stability and robustness relative to the coverage. The reconstruction performance is always significantly better at 50 per cent than at 25 per cent, but the improvement is not drastic. This suggests that a small number of visibilities can already lead to good reconstructions of the string signal.

5.3 PSM detectability threshold

In the perspective of the evaluation of the performance of the reconstruction algorithms, it is natural to ask whether the requirement for a complete reconstruction of the signal strongly limits the lowest string tension accessible in comparison with the lowest detectable string tension on the basis of the PSM.

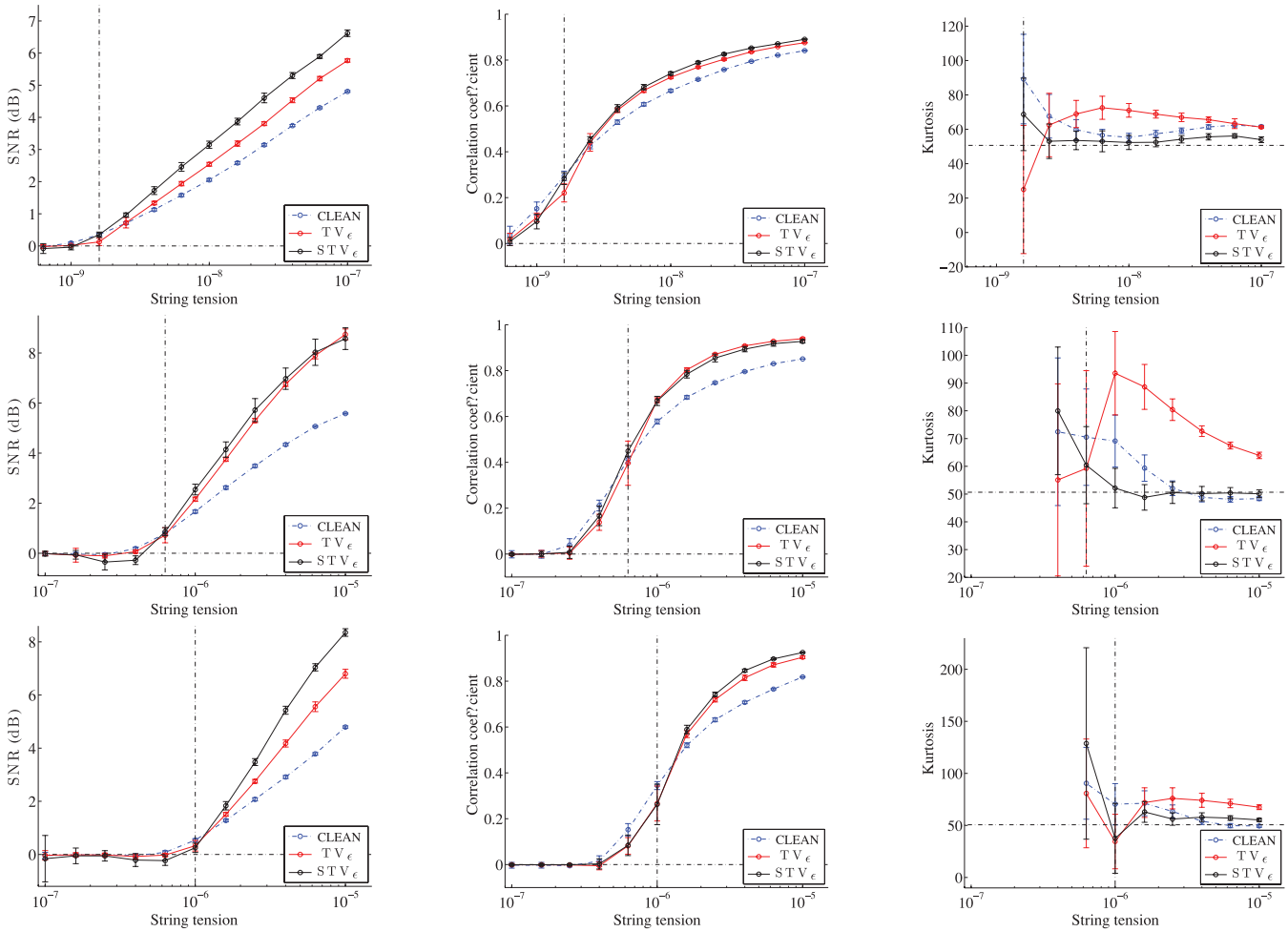

Figure 6. SNR in decibels (dB) (left-hand panels), correlation coefficient (centre panels) and kurtosis (right-hand panels) of the magnitude of the gradient of reconstructed string signals re-multiplied by the primary beam as functions of the string tension in logarithmic scaling in the range $\log_{10}\rho \in [-9, -5]$, for a coverage of 25 per cent in the noise conditions PA-IN (top panels), SA-tSZ (middle panels) and SA + tSZ (bottom panels). The reconstructions considered are those associated with CLEAN, TV$_\epsilon$ and STV$_\epsilon$. The vertical lines on the curves represent the variability at one standard deviation of the estimated statistic across the 30 test simulations considered (these lines are not visible where smaller than the width of the curves). The black dot–dashed vertical lines represent the eye visibility thresholds. The black dot–dashed horizontal lines identify either the limit of zero SNR, zero correlation coefficient or the kurtosis of the magnitude of the gradient of a string signal as expected from the test string simulation itself: $\kappa^{(\nabla Ax)} = 51$.

In this regard, for any possible string tension ρ, the probability distribution for the estimate $\widehat{\rho}$ on the basis of the PSM may be obtained from simulations. One can identify the critical value ρ_0 such that, for null string tension, the probability that the estimate $\widehat{\rho}$ is larger than ρ_0 is small: $p(\widehat{\rho} \geq \rho_0) = \alpha$, for some suitable positive value α much smaller than unity. The test for the hypothesis of null string tension is then defined as follows. For estimated values $\widehat{\rho} \geq \rho_0$, the hypothesis of null string tension may be rejected with a significance level α. On the contrary for estimated values $\widehat{\rho} < \rho_0$, the hypothesis of null string tension may not be rejected.

We define the PSM detectability threshold $\rho^\star$ such that, for the string tension $\rho^\star$, the probability that the estimate $\widehat{\rho}$ is larger than ρ_0 is large: $p(\widehat{\rho} \geq \rho_0) = 1 - \beta$, for some suitable positive value β much smaller than unity. Consequently, for string tensions larger than $\rho^\star$, the probability of rejecting a null string tension on the basis of the hypothesis test defined is larger than $1 - \beta$, called the power of the test. The value $\rho^\star$ is the smallest string tension that can be discriminated from the hypothesis of null string tension for given values of significance and power of the test. It may thus be understood as a detectability threshold determined on the basis of the PSM.

The PSM detectability thresholds in the various noise and coverage conditions considered are reported in Table 1 for $\alpha \simeq \beta \simeq 0.01$. In the noise condition PA-IN, detectability thresholds are well below the experimental upper bound, while for the noise conditions SA-tSZ and SA + tSZ they are, respectively, of the same order and larger. In all cases, the PSM detectability threshold ρ^* is only slightly below the eye visibility threshold associated with the reconstruction algorithms discussed, by a factor of smaller than 2. This discrepancy between these two thresholds confirms that the detection problem alone can be solved with the PSM only down to slightly lower string tensions than the more difficult reconstruction problem. As already emphasized in Hammond et al. (2009), it is one thing to estimate a single global parameter such as the string tension on the basis of a PSM, but quite another to explicitly reconstruct the string network itself. These comparison results are thus already very positive.

5.4 Discussion

Our results strongly support the idea of the superiority of the compressed sensing approaches for a string signal reconstruction from radio-interferometric data, in particular when specific statistical prior information is introduced in the global minimization problem defined for reconstruction. However, at the high angular resolution considered and in the noise condition SA + tSZ, the eye visibility thresholds, as well as the PSM detectability thresholds, are above the current best experimental upper bound on the string tension. One first approach to circumvent this difficulty in the perspective of the reconstruction of a possible string network from forthcoming radio-interferometric observations is to consider an observation frequency of around 217 GHz so as to eliminate the thermal SZ effect and to fall in the noise condition SA-tSZ. But even in this case, the eye visibility thresholds remain slightly higher than the experimental upper bound.

In this context, recent work by the authors might help to drastically enhance the signal reconstruction performance in the context of compressed sensing approaches (Wiaux et al. 2009b). Radio interferometers with a small field of view and baselines with a non-negligible and constant component in the pointing direction should be considered. In this context, the visibilities measured essentially identify with a noisy and incomplete Fourier coverage of the product of the planar signal multiplied by the primary beam with a linear chirp modulation. Theoretical and numerical results show the universality of the corresponding spread spectrum phenomenon relative to the sparsity basis, in terms of the achievable quality of reconstruction through global minimization problems such as TV_ϵ and STV_ϵ. Preliminary numerical results regarding the application of such a framework to the reconstruction of a string signal in the CMB look very promising.

In another line of thought, global component separation techniques might be envisaged in order to simultaneously extract all non-Gaussian components of the CMB temperature data, including the SZ effects and the string signal.

Finally, let us recall that the string signal simulations used for modelling the prior statistical distribution of the signal gradient as GGDs and for computing its power spectrum are realistic. Nevertheless, further analysis should be performed in order to study the stability of the STV_ϵ reconstruction quality relative to a discrepancy between the statistical distribution of the true signal and our model. Analysing the difference between the TV_ϵ and STV_ϵ reconstruction qualities already provides useful information in that respect, as the TV_ϵ minimization problem captures the essence of the compressibility of the signal gradient, but with a non-exact GGD shape parameter $q = 1$. In this context, one can argue in favour of a relative stability of the reconstruction quality in terms of the SNR and correlation coefficient as these measures are indeed smaller for TV_ϵ than for STV_ϵ, but still larger than for CLEAN. This stability is lost in terms of the kurtosis though.

6 CONCLUSION

The STV_ϵ algorithm proposed for the reconstruction of a string signal from arcminute resolution radio-interferometric data of the CMB is designed in the framework of compressed sensing. It notably relies on a model of the prior statistical distribution of the signal, fitted on the basis of realistic simulations. The algorithm shows superior performance relative to the standard CLEAN algorithm. Secondary CMB anisotropies strongly hamper the signal reconstruction though, and further work is still required in order to obtain good performance at string tensions below the current experimental upper bound.

ACKNOWLEDGMENTS

The authors wish to thank M. J. Fadili for private communication of results on optimization by proximal methods. The authors also thank A. A. Fraisse, C. Ringeval, D. N. Spergel and F. R. Bouchet for kindly providing simulations of a string signal. The authors also thank the reviewer for his valuable comments. YW is Postdoctoral Researcher of the Belgian National Science Foundation (F.R.S.-FNRS).

REFERENCES

Albrecht A., Turok N., 1985, Phys. Rev. Lett., 54, 1868
Albrecht A., Turok N., 1989, Phys. Rev. Lett., 40, 973
Allen B., Shellard E. P. S., 1990, Phys. Rev. Lett., 64, 119
Amsel S., Berger J., Brandenberger R. H., 2008, J. Cosmol. Astropart. Phys., 04, 015
Baraniuk R., 2007, IEEE Signal Processing Magazine, 24, 118
Barker R. et al., 2006, MNRAS, 369, L1
Bennet D. P., 1986, Phys. Rev. D, 33, 872
Bennet D. P., Bouchet F. R., 1989, Phys. Rev. Lett., 63, 2776
Bennet D. P., Bouchet F. R., 1990, Phys. Rev. D, 41, 2408
Bennett C. L. et al., 2003, ApJS, 148, 1
Bevis N., Hindmarsh M., Kunz M., 2004, Phys. Rev. D, 70, 043508
Bevis N., Hindmarsh M., Kunz M., Urrestilla J., 2007, Phys. Rev. D, 75, 065015
Blythe J. H., 1957, MNRAS, 117, 644
Bouchet F. R., Bennet D. P., Stebbins A., 1988, Nat, 335, 410
Candès E. J., 2006, in Sanz-Solé M., Soria J., Varona J. L., Verdera J., eds, Proc. Int. Congress Math. Vol. 3. Euro. Math. Soc., Zürich, p. 1433
Candès E. J., 2008, Comptes Rendus Acad. Sci., 346, 589
Candès E. J., Romberg J., Tao T., 2006a, IEEE Trans. Inf. Theory, 52, 489
Candès E. J., Romberg J., Tao T., 2006b, Commun. Pure Appl. Math., 59, 1207
Combettes P. L., Pesquet J.-C., 2007, IEEE Sel. Top. Signal Processessing, 1, 564
Danos R. J., Brandenberger R. H., 2008, preprint (arXiv:0811.2004)
Davis A. C., Kibble T. W. B., 2005, Contemporary Phys., 46, 313
Donoho D. L., 2006, IEEE Trans. Inf. Theory, 52, 1289
Donoho D. L., Tanner J., 2009, J. Am. Math. Soc., 22, 1
Fadili M. J., Starck J.-L., 2009, in Proc. IEEE Int. Conf. Image Process (ICIP). IEEE Signal Process. Soc., in press
Fraisse A. A., 2007, J. Cosmol. Astropart. Phys., 03, 008
Fraisse A. A., Ringeval C., Spergel D. N., Bouchet F. R., 2008, Phys. Rev. D, 78, 043535
Gott J. R., 1985, ApJ, 288, 422
Hammond D. K., Wiaux Y., Vandergheynst P., 2009, MNRAS, 398, 1317
Hindmarsh M., 1995, Nucl. Phys. Proc. Suppl., 43, 50
Hindmarsh M., Kibble T. W. B., 1995, Rep. Prog. Phys., 58, 477
Hinshaw G. et al., 2007, ApJS, 170, 288
Hinshaw G. et al., 2009, ApJS, 180, 225
Högbom J. A., 1974, A&AS, 15, 417
Jeong E., Smoot G. F., 2005, ApJ, 624, 21
Jones M. E., 2002, in Chen L.-W., Ma C.-P., Ng K.-W., Pen U.-L., eds, ASP Conf. Ser. Vol. 257, AMiBA 2001: High-z Clusters, Missing Baryons, and CMB Polarization. Astron. Soc. Pac., San Francisco, p. 35
Kaiser N., Stebbins A., 1984, Nat, 310, 391
Kibble T. W. B., 1985, Nucl. Phys. B, 252, 227
Komatsu E., Seljak U., 2002, MNRAS, 336, 1256
Komatsu E. et al., 2009, ApJS, 180, 330
Kosowsky A., 2006, New Astron. Rev., 50, 969

Lo A. S., Wright E. L., 2005, BAAS, 37, 1429
Mallat S. G., 1998, A Wavelet Tour of Signal Processing. Academic Press, San Diego
Mallat S. G., Zhang Z., 1993, IEEE Trans. Signal Processing, 41, 3397
Moessner R., Perivolaropoulos L., Brandenberger R., 1994, ApJ, 425, 365
Moreau J. J., 1962, A&A, 255, 2897
Perivolaropoulos L., 1993, Phys. Lett. B, 298, 305
Rocha G., Hobson M. P., Smith S., Ferreira P., Challinor A., 2005, MNRAS, 357, 1
Ryle M., Hewish A., 1960, MNRAS, 120, 220
Ryle M., Vonberg D. D., 1946, Nat, 158, 339
Ryle M., Hewish A., Shakeshaft J. R., 1959, IRE Trans. Antennas Propagation, 7, 120
Schwarz U. J., 1978, A&A, 65, 345
Spergel D. N. et al., 2003, ApJS, 148, 175
Spergel D. N. et al., 2007, ApJS, 170, 377
Sunyaev R. A., Zel'dovich Y. B., 1980, ARA&A, 18, 537
Thompson A. R., Moran J. M., Swenson G. W. Jr, 2004, Interferometry and Synthesis in Radio Astronomy. Wiley-VCH Verlag GmbH & Co. KGaA, Weinheim
Turok N., Spergel D. N., 1990, Phys. Rev. Lett., 64, 2736
Vachaspati T., Vilenkin A., 1984, Phys. Rev. D, 30, 2036
van den Berg E., Friedlander M. P., 2008, SIAM J. Sci. Comput., 31, 890
Vilenkin A., Shellard E. P. S., 1994, Cosmic Strings and Other Topological Defects. Cambridge Univ. Press, Cambridge
Wiaux Y., Jacques L., Puy G., Scaife A. M. M., Vandergheynst P., 2009a, MNRAS, 395, 1733
Wiaux Y., Puy G., Boursier Y., Vandergheynst P., 2009b, MNRAS, 400, 1029
Wyman M., Pogosian L., Wasserman I., 2005, Phys. Rev. D, 72, 023513
Wyman M., Pogosian L., Wasserman I., 2006, Phys. Rev. D, 73, 089905(E)
Zwart J. T. L. et al., 2008, MNRAS, 391, 1545

This paper has been typeset from a TEX/LATEX file prepared by the author.